High-Rate Electroreduction of Carbon Monoxide to Multi-Carbon Products

Matthew Jouny, Wesley Luc, and Feng Jiao*

Center for Catalytic Science and Technology, Department of Chemical and Biomolecular Engineering, University of Delaware, Newark, DE 19716 USA

*Corresponding author: jiao@udel.edu

Abstract

Carbon monoxide electrolysis has previously been reported to yield enhanced multi-carbon (C_{2+}) Faradaic efficiencies up to ~55% but only at low reaction rates. This is due to the low solubility of CO in aqueous electrolytes and operation in batch-type reactors. Here we present a high-performance CO flow electrolyzer with a well-controlled electrode-electrolyte interface that can reach total current densities up to 1 A/cm^2 together with improved C_{2+} selectivities. Computational transport modelling and isotopic $C^{18}O$ reduction experiments suggest the enhanced activity is due to a higher surface pH under CO reduction conditions, which facilitated the production of acetate. At optimal operating conditions, we achieve a C_{2+} Faradaic efficiency of ~91% with a C_{2+} partial current density over 630 mA/cm^2. Further investigations show that maintaining an efficient triple-phase boundary at the electrode-electrolyte interface is the most critical challenge to achieving a stable CO/CO_2 electrolysis process at high rates.

Introduction

The rapid development of novel energy technologies has decreased renewable electricity prices significantly over the past decade. For example, the photovoltaic industry has consistently made strides on improving solar cell efficiencies and reducing manufacturing costs with a projected electricity price as low as \$0.03/kWh by 2030.[1] This foreseen cheap electricity has motivated significant research interest in the development of electrified pathways for chemical and fuel production. Compared to traditional chemical processes driven by fossil energy, electrochemical processes are often more environmentally friendly, can operate under relatively mild conditions, and can also be coupled with renewable electricity sources at remote locations.[2-4] The electrolysis of carbon dioxide (CO_2) has attracted significant attention as a process to produce high-value chemicals such as ethylene and ethanol, but current state-of-the-art CO_2 electrolyzers generally suffer from low selectivity and high overpotentials at practical reaction rates (>300 mA/cm^2).[5-7]

As an alternative to direct CO_2 electrolysis, a two-step cascade process where CO_2 is initially reduced to carbon monoxide (CO) and then sequentially reduced to multi-carbon (C_{2+}) products holds several advantages. As CO is widely accepted as a key reaction intermediate for C-C coupling in carbon dioxide reduction (CO_2R),[8] directly feeding CO as the reactant into a CO electrolyzer to increase the near-surface CO concentration (and consequently *CO surface coverage) may significantly enhance the performance toward producing C_{2+} products.[9,10] Furthermore, CO reduction (COR) can be done in alkaline electrolytes that suppress the competitive hydrogen evolution reaction, improve charge transfer kinetics, and boost selectivity towards C_{2+} products,[11-13] without the significant carbonate formation that plagues CO_2 reduction.[14] Finally, while a cascade process would require an additional gas separation step to purify the CO feed, this is likely to be minor relative to the total system economics.[15]

Copper is currently being extensively studied as it is the only monometallic CO_2/CO reduction catalyst that can produce C_{2+} hydrocarbons and oxygenates with appreciable selectivities. The majority of research efforts have primarily focused on particle size effects,[16-18] nanostructuring,[19-22] facet dependency,[10,23,24] bimetallic alloys,[25-29] and surface modification.[30-34] In particular, "oxide-derived" copper (OD-Cu) has shown significant COR selectivities towards ethanol and acetate at low overpotentials.[35-37] To date, most COR investigations were performed in a batch-type electrochemical cell configuration, where mass transport limitations arise due to the extremely low solubility of CO in aqueous electrolytes such as KOH solution.[38] Consequently, high oxygenate Faradaic efficiency up to 70% has been demonstrated, but only at very low reaction rates (~1 mA/cm^2). In order to circumvent mass transport limitations, a flow cell reactor can be engineered where the gaseous reactant is directly fed to the electrode-electrolyte interface to form a triple-phase boundary such that high rates of COR can be achieved. However, to the best of our knowledge, a flow system that can achieve high rates for COR has yet to be demonstrated in the literature.

Herein, we constructed a three-compartment CO flow electrolyzer in which a hydrophobic porous carbon support was loaded with a copper catalyst and positioned between a gas and liquid chamber where CO is directly fed on one side while electrolyte was fed on the other (Figure 1a). The well-engineered electrode-electrolyte interface (Figure 1b) allowed us to convert CO at high reaction rates with a remarkable C_{2+} selectivity. At the optimal conditions, the flow cell utilizing an OD-

Cu catalyst exhibited a 91% C_{2+} selectivity at a partial current density of 635 mA/cm^2, representing the highest performance that has ever been achieved for COR. Further studies revealed that maintaining an efficient electrode-electrolyte interface where gaseous reactant/products can easily transport in/out of the porous electrode without disrupting ionic and electrical conductivity is crucial for a stable performance at high reaction rates. Additionally, we compared CO_2R and COR performances in an identical setup and demonstrated that CO reduction has multiple advantages over CO_2 reduction in a flow cell configuration, such as a higher C_{2+} selectivity and a more robust interface. Finally, surface pH calculations under COR and CO_2R conditions and isotopic labelling studies suggest that the higher surface pH for COR facilitates the improved activity as well as acetate production.

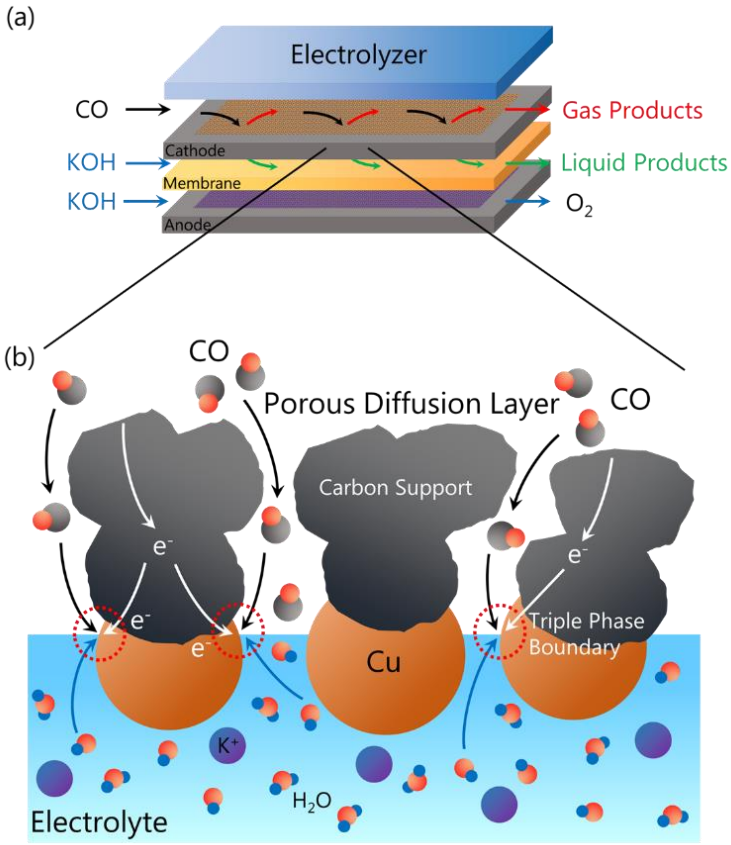

Figure 1-Flow Electrolyzer Schematic: (a) A schematic of the three-compartment microfluidic CO flow electrolyzer and (b) a schematic of the well-controlled electrode-electrolyte interface for CO reduction at high current densities.

Results

Catalyst characterization and COR performance

OD-Cu catalyst was prepared following a literature procedure where Cu particles were annealed in air, followed by an *in-situ* electrochemical reduction treatment.[35] In a typical preparation, commercial Cu particles ("micron Cu") with an average particle size of 0.5-1.5 μm (Figure 2a) were first annealed at 500 ^oC for 2 hours. After annealing, a clear morphology change from spherical particles to irregular particles (0.1 to 1 μm) was observed and a typical scanning electron microscopy (SEM) image is shown in Supplementary Fig. 1. Structural characterizations using

powder X-ray diffraction (XRD) technique revealed a phase transition from cubic metallic Cu into monoclinic CuO (Figure 2c), which is consistent with X-ray photoelectron spectroscopy (XPS) results (Figure 2d). The resulting CuO particles were dispersed in a catalyst ink with a small amount of multi-walled carbon nanotubes and dropcast onto a gas-diffusion layer (GDL) with a final catalyst loading of ~1 mg/cm^2. The electrode was then pre-conditioned through an *in-situ* electrochemical reduction at a constant current density of 15 mA/cm^2. After the pre-conditioning, the OD-Cu sample became highly porous with a pore size of 10-20 nm (Figures 2b and Supplementary Fig. 2). *In-situ* X-ray absorption spectroscopy (XAS) under COR conditions (5 mA/cm^2 in 0.1M KOH) in a custom-built H-cell (Supplementary Fig. 3) indicates that the catalyst is metallic Cu^0 after pre-reduction and under reaction conditions (Supplementary Fig. 4). The micron Cu electrodes were prepared using the same commercial Cu powder and the spherical morphology of the particles was maintained throughout the preparation procedure (Supplementary Fig. 5).

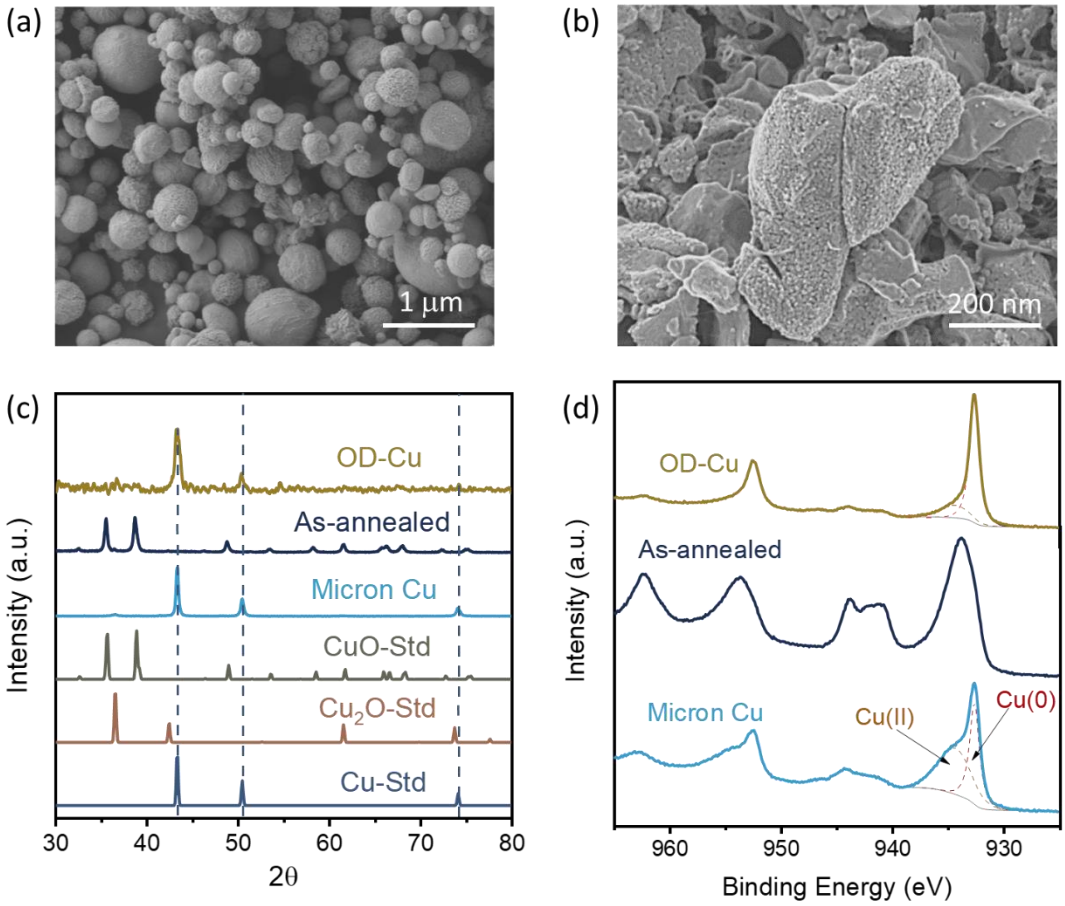

Figure 2-Catalyst Structural Characterization: (a) SEM image of commercial copper powder (Micron Cu), (b) SEM image of oxide-derived copper (OD-Cu) particles on GDL, (c) XRD of copper samples, and (d) XPS of copper samples. Data for copper standards are also showed in (c) for comparison.

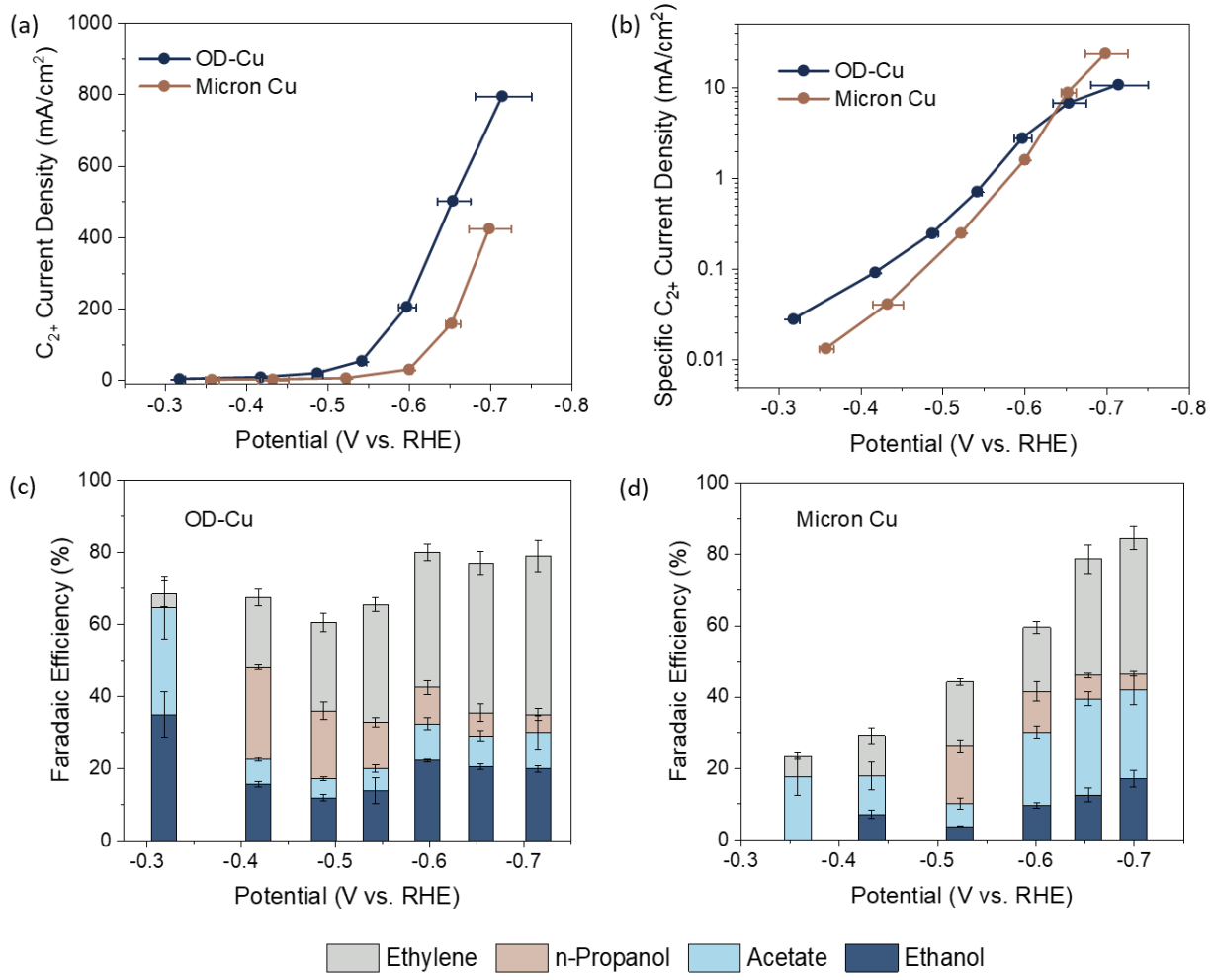

Figure 3-COR performance of OD-Cu and Micron Cu: Partial current density for C_{2+} products vs. applied potential for CO reduction in 1M KOH on OD-Cu and micron Cu normalized to (a) geometric surface area and (b) electrochemical surface area, with corresponding Faradaic efficiency profiles for (c) OD-Cu and (d) micron Cu. Error bars represent the standard deviation from at least three independent measurements.

The COR activities of both OD-Cu and micron Cu electrodes were evaluated using a three-compartment flow electrolyzer (Figure 1a). The COR results are summarized in Figure 3 and the products detected in significant quantities were ethanol, acetate, ethylene, and n-propanol, with the remaining charge attributed to the competing hydrogen evolution reaction. For both OD-Cu and micron Cu electrodes, there was a near exponential increase in the CO reduction current density with respect to applied potential (Figure 3a), indicating excellent transport of CO to the catalytic surface at the triple-phase boundary. Furthermore, a remarkable partial current density for C_{2+} products (830 mA/cm^2) was obtained using OD-Cu at a moderate applied potential (-0.72 V vs. RHE). To compare the reaction rates of both Cu electrodes, the performance was normalized to the electrochemical surface area (ECSA, see Supplementary Fig. 6 for measurement). The OD-Cu copper electrode exhibited higher geometric and ECSA-corrected C_{2+} current densities than micron Cu at lower overpotentials (Figures 3a-b). The enhanced activity of OD-Cu for COR in batch systems at low overpotentials has been attributed to the presence of grain boundaries,[35,38-41]

or other unique Cu facets.[37,42] However, copper can undergo significant surface restructuring under a CO-rich environment,[43-45] and future work involving advanced *operando* techniques mirroring flow cell conditions is needed to elucidate true structure-property relationships. The non-linearity of Figure 3b at high overpotentials is likely caused by mass transport limitations of the product gas bubbles which begin to block the catalyst at high current densities (>500 mA/cm^2). The two electrodes exhibited similar normalized total current densities (Supplementary Fig. 7). After a 1-hour constant current density electrolysis at 500 mA/cm^2, the morphology of the OD-Cu particles was maintained (Supplementary Fig. 8).

At low overpotentials, OD-Cu showed significantly higher C_{2+} Faradaic efficiencies (69%, Figure 3c) at -0.32V vs. RHE than what were observed with micron Cu (Figure 3d). At -0.42V vs. RHE, the OD-Cu exhibited a 26% Faradaic efficiency towards n-propanol, which is the highest value reported for CO_2/CO electrolysis in the literature. As the overpotential increased, the OD-Cu began to produce significant amounts of ethylene with the total oxygenates Faradaic efficiency remaining constant at ~40%, whereas the Faradaic efficiency towards n-propanol declined to ~6%. We attribute this to the rate of the C-C coupling reaction (which may be a thermochemical reaction step) for n-propanol formation becoming relatively slow compared to the C_2 intermediate protonation reaction at high overpotentials.[46] Interestingly, the micron Cu electrode showed a similar C_{2+} selectivity profile at high overpotentials, with a total C_{2+} Faradaic efficiency of ~80%. This demonstrates that polycrystalline copper exhibits similar selectivity as OD-Cu for COR to C_{2+} products at high overpotentials.

Comparison between COR and CO_2R

To further illustrate the advantages of CO electrolysis over CO_2 electrolysis for C_{2+} production, we operated the flow electrolyzer using 1 M KOH electrolyte, while switching the gas feed between CO and CO_2 during a constant current electrolysis at 300 mA/cm^2 on OD-Cu and micron Cu. Products were sampled after 20 minutes to ensure that steady-state was reached. Figures 4a-b show the total cell voltage and Faradaic efficiencies over time. Remarkably, the overall C_{2+} Faradaic efficiency for COR (~80%) is much higher than that of CO_2R (~55%), as CO_2 reduction produced significant amounts of CO (~15%) and $HCOO^-$ (~7%) that were not counted for the total C_{2+} Faradaic efficiency. Furthermore, for the same C_{2+} products, COR requires 1/3 less electrons than CO_2R. As a result, the molar production rate of C_{2+} products were more than doubled for COR (Supplementary Figs. 9 and 10).

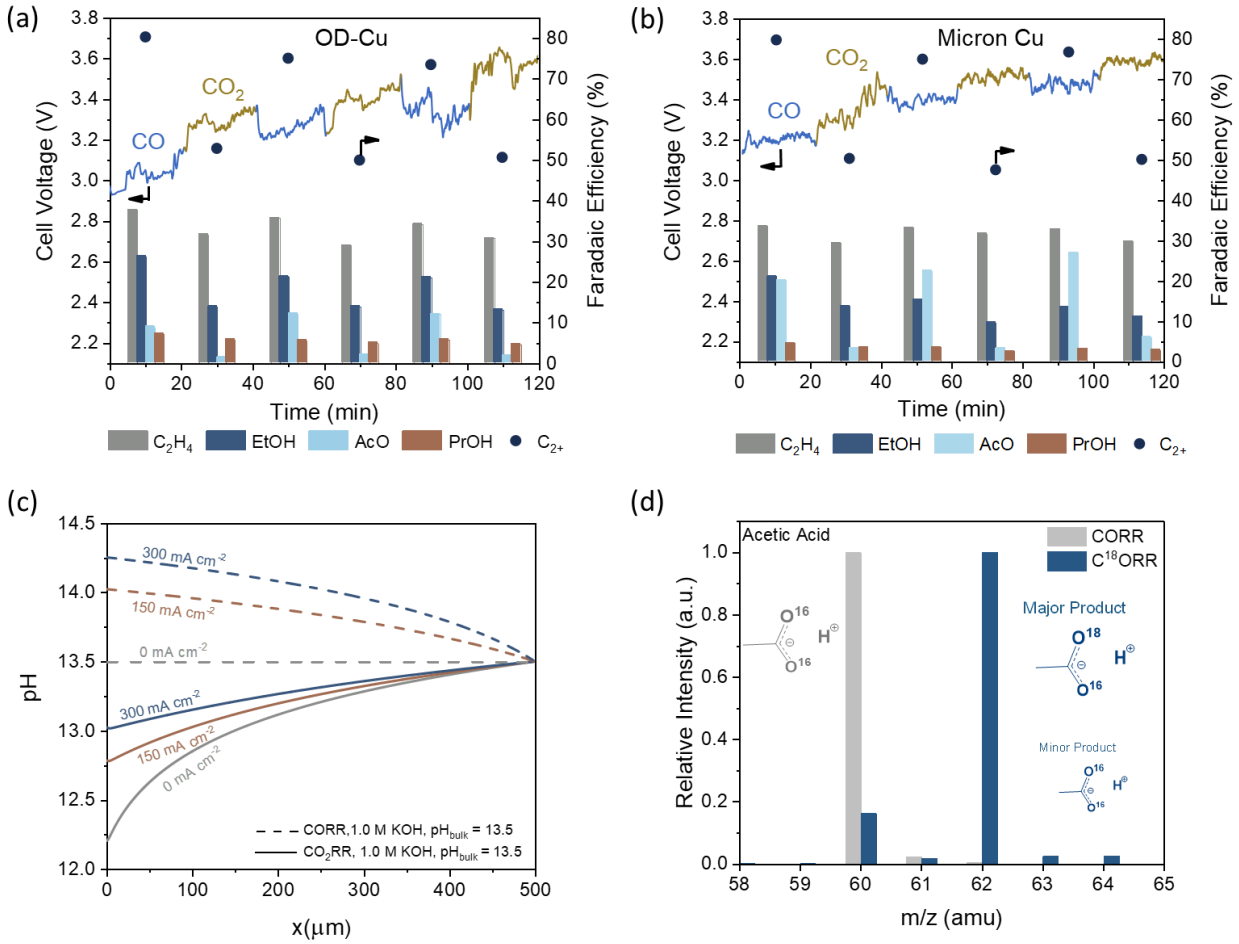

Figure 4-Comparison of CO_2R and COR performance: (a) CO/CO_2 reduction on OD-Cu at 300 mA/cm^2 in 1M KOH over two hours showing the difference in C_{2+} product selectivities, (b) CO/CO_2 reduction on micron Cu at 300 mA/cm^2 in 1M KOH over two hours showing the difference in C_{2+} product selectivities, (c) calculated pH profiles for CO/CO_2 reduction in 1M KOH under various current densities, and (d) mass spectrum of partially labelled acetic acid produced by $C^{18}O$ reduction at 300 mA/cm^2 in 1M KOH.

Additionally, the overall cell voltage increased by ~100 mV when the gas feed was changed from CO to CO_2. The increase in cathodic overpotential could either be a result of the additional energy required to activate CO_2 relative to CO or a pH decrease at the electrode-electrolyte interface. The latter would likely be caused by carbonate formation through a fast chemical reaction between CO_2 and KOH, which served as a buffer layer and inevitably lowers the pH near the catalytic surface.[14] Since carbonate has a lower ionic conductivity than KOH, this would lead to an increase in the cathodic overpotential.

In order to better understand the difference in interfacial pH between CO_2R and COR, we modelled the transport of CO_2/CO between the electrode-electrolyte interface and bulk electrolyte (see Supplementary Methods for details).[13,47] The pH gradients for CO_2/CO reduction under various current densities are shown in Figure 4c. In the case of CO_2 reduction at 0 mA/cm^2, there is already a significant reduction in surface pH (x = 0 μm) due to the fast equilibrium reaction between CO_2

and KOH. However, the surface pH increases with increasing current density in both CO_2 and CO reduction cases due to the generation of OH^- ions. At 300 mA/cm^2, the estimated OH^- concentration under CO reduction conditions is more than 1 order of magnitude higher than under CO_2 reduction conditions. It should also be noted that previous studies of CO_2 electrolysis using KOH as the electrolyte in a flow electrolyzer often assumed a pH value based on the bulk KOH concentration, leading to an underestimation of the electrode overpotential for CO_2 reduction in alkaline electrolyte.[48,49]

Another observation from Figures 4a-b is that the selectivity for ethylene, ethanol, and n-propanol did not change significantly before and after the CO/CO_2 switch, while the acetate Faradaic efficiency was much higher for COR and thus the major contributor to the C_{2+} selectivity difference between CO and CO_2 reduction. Mechanistically, the formation of acetate from CO_2/CO reduction is poorly understood. Li and Kanan suggested that acetate formation is due to hydroxide attack of a surface intermediate due to observed increase in acetate FE at higher KOH concentrations.[35] Moreover, Koper *et al.* recently reported a favourable acetate formation at high pH in CO_2 reduction due to the hydroxide ions promoted Cannizzaro-type reactions at the catalytic surface.[50] However, the molar ratios of the produced ethanol and acetate are not equivalent (Supplementary Figs. 9 and 10), indicating there may be an additional pathway to acetate. Garza *et al.* also proposed a direct reduction of CO to acetate without oxygen donation from the electrolyte through the isomerization of *OCH_2COH to a three-membered ring attach to the surface.[51]

$C^{18}O$ isotopic labelling studies

To further gain mechanistic insights into the formation of acetate, isotopic labelled $C^{18}O$ (Sigma Aldrich, 95 at% ^{18}O) was fed to the electrolyzer at a constant current of 300 mA/cm^2 and a gas chromatography-mass spectrometry (GC-MS) system was used to analyze the liquid products. We note that this investigation can only be done with labelled $C^{18}O$ rather than $C^{18}O_2$ due to the rapid equilibrium exchange of oxygen atoms when CO_2 reacts with KOH. Furthermore, the use of the flow cell allows for easy quantification of labelled products due to the rapid production of concentrated products that would otherwise not be possible with a batch-type reactor. The liquid products were acidified with hydrochloric acid to a pH value of ~2 after electrolysis before injecting into the GC-MS to enable acetate detection as acetic acid. If the acetate is formed through an oxygen donation from the electrolyte, it should only be partially labelled (62 amu), while a direct reduction pathway would yield fully labelled acetate (64 amu).

The mass fragmentation patterns of acetic acid produced from unlabelled CO and labelled $C^{18}O$ are shown in Figure 4d. The parent ion of acetic acid (60 amu) produced from unlabelled CO matches well to that of the NIST database. A clear mass shift by 2 amu (62 amu) was observed when labelled $C^{18}O$ was used, which indicates that only one oxygen of acetic acid is labelled. A small signal at 60 amu is likely due to $C^{16}O$ impurity in the feed. Since the signal at 64 amu, as well as at 63 amu, is even smaller than the observed signal at 60 amu, we attribute this signal to the natural isotope abundance of ^{13}C, and not acetic acid with both oxygen atoms labelled. Additionally, the signal ratio between 62 and 60 amu is close that of the ratio of ^{18}O and ^{16}O in the gas feed; and therefore, we conclude that the observed acetic acid with a signal at 62 amu consisted of one oxygen originating from labelled $C^{18}O$ and one oxygen originating from the electrolyte,

most likely from a OH^- ion reacting with an intermediate species. Combining these observations with the estimated pH gradients shown in Figure 4c, we attribute the high acetate selectivity in COR to a higher local pH at the electrode-electrolyte interface, where the abundance of OH^- ions near the catalytic surface can easily react with an intermediate to form acetate. A proposed pathway to acetate is shown in Supplementary Fig. 11. However, we note that other effects such as the presence of carbonates under CO_2R conditions may also influence the selectivity.

In addition to acetic acid, we also detected ethanol and n-propanol via GC-MS along with a small amount of acetaldehyde. Surprisingly, acetaldehyde was entirely unlabelled, and ethanol/n-propanol were only partially labelled (Supplementary Fig. 12). The unlabelled acetaldehyde can be explained by the rapid oxygen exchange between acetaldehyde and water which has been extensively studied by Greenzaid et al.[52] This was verified by adding 0.2% of acetaldehyde, ethanol, and acetic acid to 98% $H_2{}^{18}O$. Indeed, a clear mass shift by 2 amu (46 amu) was observed with acetaldehyde; however, no oxygen exchange was observed with ethanol or acetic acid (Supplementary Fig. 13). Therefore, the observation of only partially labelled ethanol and n-propanol is likely due to acetaldehyde oxygen exchange prior to further reduction, since acetaldehyde has been shown to be a reaction intermediate to these alcohols.[36] Overall, this demonstrates the challenges of gaining mechanistic insights through isotopic labelled oxygen studies for CO reduction, and future work such as direct sampling at the reaction interface through differential electrochemical mass spectrometry (DEMS) is required.[53]

Influence of KOH concentration on COR performance

The pH effect on CO reduction was further studied by varying the KOH electrolyte concentration from 0.1M to 2.0 M. The cathode polarization curves for C_{2+} products in 0.1M, 0.5 M, 1.0M, and 2.0 M KOH aqueous electrolytes are shown in Figure 5a. Both C_{2+} partial current density and Faradaic efficiency increased (Figures 5a-b) as the KOH concentration increased. While the HER partial current density also increased with increasing concentration, the HER Faradaic efficiency was dramatically reduced (Supplementary Fig. 14). We attribute this enhancement to two effects: 1) the reduction of charge transfer resistance across the electrolyte that improved the active area of the triple-phase boundary due to the increase in electrolyte conductivity at higher concentrations,[11,54] and 2) higher pH at the electrocatalytic interface that favours C-C coupling. Although previous studies on CO reduction were primarily carried out in a 0.1 M KOH electrolyte, recent computational work have suggested that a high pH environment could enhance C-C coupling through the dimerization of adsorbed CO.[12]

As reflected, Figures 5a-b clearly shows that high KOH concentrations are favourable for CO reduction to C_{2+} products (see Supplementary Table 1 for specific product Faradaic Efficiencies). The molar production ratio of acetate to other products generally increased with increasing KOH concentration (Supplementary Fig. 15), further supporting that OH^- ions shift selectivity to acetate. In 1.0 M KOH electrolyte, we achieved a C_{2+} partial current density of 829 mA/cm^2 with a total C_{2+} Faradaic efficiency of 79% at a moderate potential of -0.72V vs. RHE. At a slightly lower potential (-0.67V vs. RHE) in 2.0M KOH, a C_{2+} partial current density of 635 mA/cm^2 with a total C_{2+} Faradaic efficiency of 91% was obtained. In terms of C_{2+} current density and Faradaic efficiency, our results are significantly better than performances reported in the current state-of-the-art CO_2R (Figure 5c, see Supplementary Table 2 for details).[13,22,24,30-33,49,55-60]

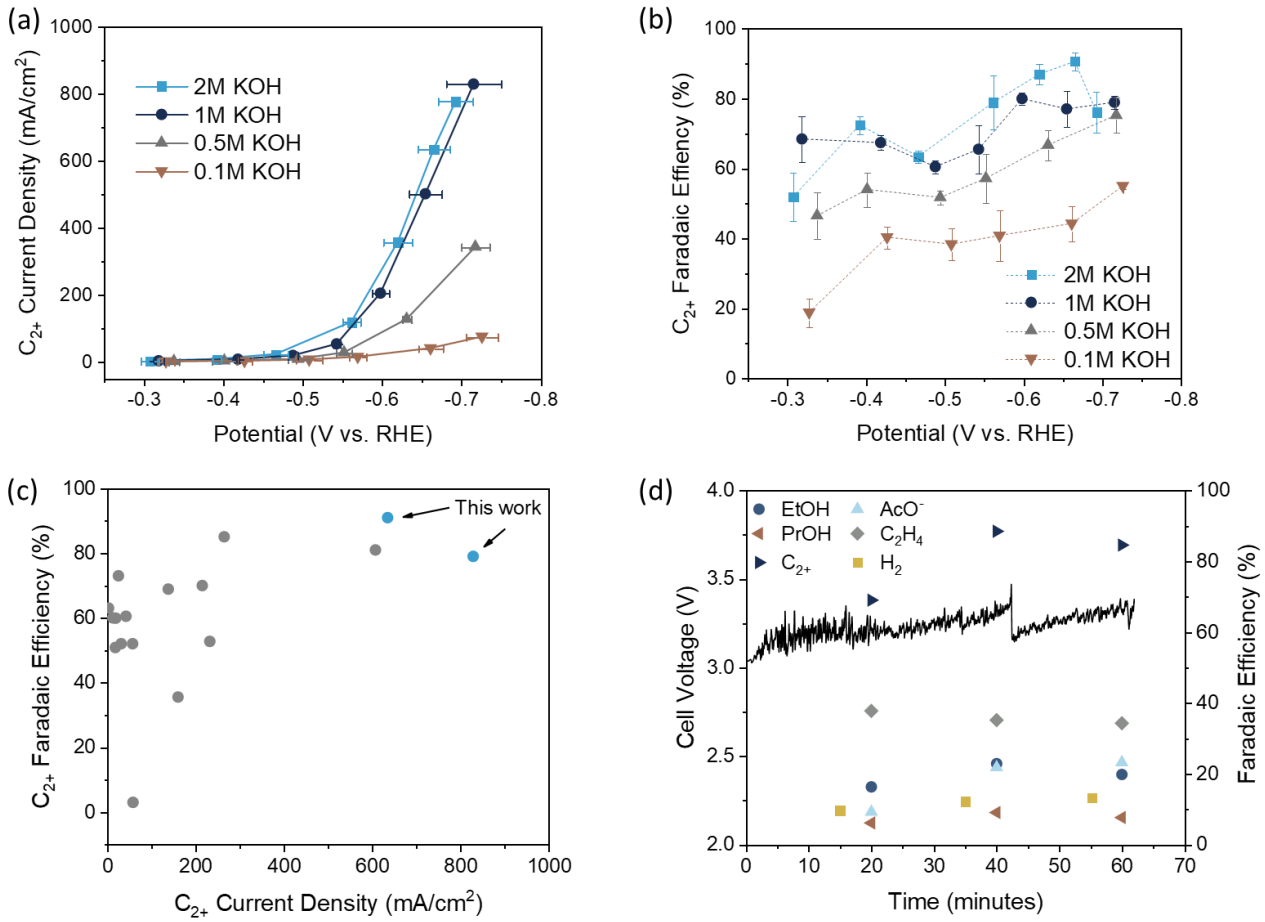

Figure 5-KOH concentration effect on COR performance: (a) partial current density for C_{2+} products for CO reduction in varying concentrations of KOH and (b) associated Faradaic efficiencies, (c) comparison of the partial current densities and Faradaic efficiencies for C_{2+} products reported in this work compared to current state-of-the-art, (d) cell voltage and Faradaic efficiencies for CO reduction on OD-Cu in 2M KOH at 500 mA/cm^2 over 1 hour. Error bars represent the standard deviation from at least three independent measurements.

The stability of the CO electrolyzer was also examined at a constant current of 500 mA/cm^2 with 2.0 M KOH electrolyte in a two-electrode flow cell configuration. The applied cell voltage increased from 3.05 V to 3.25 V over the course of 1-hour electrolysis with gradual increases and sudden decreases (Figure 5d), which was caused by the gradual build-up of gas bubbles in the liquid catholyte chamber until it was flushed out at once. Despite this, a 1-hour stable performance was achieved at a cell potential of ~3.2V and a current density of 500 mA/cm^2. The slight decrease of total C_{2+} Faradaic efficiency after 30 minutes is predominantly due to flooding issues through the GDL into the CO gas chamber, which was caused by the condensation of water vapour. At such a high current density, water quickly accumulated in the gas chamber and caused cell voltage increase and fluctuations (Figure 5d). In the case of CO_2 reduction, the same water accumulation issue also existed, but much worse stability was observed (Supplementary Fig. 16). This severe degradation was likely due to carbonate formation at the electrode-electrolyte interface that blocks

the pores of the GDL.[14] Attempts to obtain higher C_{2+} partial current from CO reduction at higher cell voltages were made and a total current density beyond 1 A/cm^2 was achieved; however, the cell performance was only maintained for less than 30 minutes because of severe flooding issues into the gas chamber. Clearly, maintaining an efficient three-phase boundary at the electrode-electrolyte interface is crucial to obtaining a high-performing CO electrolyzer that can be operated at extremely high current densities while preserving a high C_{2+} selectivity.

Discussion

While we have successfully demonstrated a CO electrolyzer that can operate at high rates with a remarkable C_{2+} selectivity, some critical challenges must be addressed before this technology can be commercialized. The CO flow electrolyzer was operated at ~3.2 V which is ~2.1 V above the thermodynamic potential, resulting in an energetic efficiency of < 40%. Consequently, the low energetic efficiency will significantly increase the cost associated with electricity consumption and reduce the profitability of the whole process. For the CO electrolyzer cell presented in this work, the resistance between the cathode and anode was ~1.5 Ohm, corresponding to a resistive loss of about 0.75 V (at 500 mA/cm^2). The voltage loss associated with internal resistance could be reduced by depositing the anode catalyst directly on the membrane and using a more conductive anion exchange membrane. Maintaining a stable cell operation over a long period of time is also important. Flooding and salt accumulation issues at the electrode-electrolyte interface must be addressed through interface engineering. For example, Dinh et al. recently demonstrated excellent stability for CO_2 reduction using custom-designed gas diffusion electrodes.[13] Additionally, the flow cell suffered from a low single-pass conversion of CO gas feed, which would lead to a high cost to separate gas products from the unreacted CO reactant.

In summary, despite the remaining process engineering challenges, we have demonstrated a CO flow electrolyzer that can achieve over 630 mA/cm^2 with a C_{2+} selectivity above 90%, exceeding the performance for the current state-of-the-art COR and CO_2R systems. The flow electrolyzer design successfully overcame mass transport limitations associated with the low solubility of CO in aqueous electrolytes and allowed us to achieve superior performances at high rates. This work also illustrated the critical need to design a robust electrode-electrolyte interface, which allowed us to investigate COR and CO_2R at practical reaction rates. The comparison between COR and CO_2R clearly demonstrated the potential advantages of CO electrolysis over CO_2 electrolysis to produce valuable C_{2+} chemicals. With a CO_2-derived CO source or other CO-rich sources, CO electrolysis technology may be considered as an alternative approach to produce high-value C_{2+} chemicals in practical applications.

Methods

Preparation of Electrodes

Commercial copper powder (0.5-1.5 μm, 99%) was purchased from Alfa Aesar and stored under Ar atmosphere. 1 g of copper powder was placed in a ceramic crucible and immediately heated to 500 ^{o}C for 2 hours. Following thermal annealing, the copper powder sintered into a black sheet, which was hand ground to form a fine powder. 100 mg of powder was mixed with 0.5 mL tetrahydrofuran containing 0.5 mg/mL multiwalled carbon nanotubes (>98% carbon basis, O.D. ×

L 6-13 nm × 2.5-20 μm, Sigma Aldrich), 2 mL of isopropanol, and 20 μL of Nafion ionomer solution (10 wt% in H_2O). The oxide-derived copper (OD-Cu) electrode was prepared via in-situ electrochemical reduction at a constant current density of 15 mA/cm^2. An identical ink was prepared using the as-purchased commercial micron copper. The catalyst inks were sonicated for 30 minutes and then dropcast onto a Sigracet 29 BC gas diffusion layer (GDL, Fuel Cell Store) to a loading of 1 mg/cm^2. IrO_2 anodes were prepared by mixing 50 mg IrO_2 nanoparticles (99%, Alfa Aesar) with 0.5 mL of DI H_2O, 2 mL of isopropanol, and 20 μL of Nafion ionomer solution (10 wt% in H_2O), which was sonicated and dropcast onto Sigracet 29BC GDL at 1 mg/cm^2 loading. A fresh cathode was used for each flow cell experiment, while anodes were reused 3 times.

Materials Characterization

Scanning electron microscopy (SEM) images were obtained on an Auriga 60 Crossbeam. X-ray diffraction (XRD) was performed on a Bruker D8 Discovery diffractometer using a Cu Kα radiation source. A Thermo Scientific K-Alpha X-ray Photoelectron Spectrometer (XPS) System was used to analyse the surface composition near the surface. XPS fitting was conducted with CasaXPS software with the adventitious carbon peak being calibrated to 284.5 eV. All peaks were fitted using a Gaussian/Lorentzian product line shape and a Shirley background.

The electrochemical surface area (ECSA) was determined by measuring the double-layer capacitances of the commercial micron Cu and OD-Cu and comparing to a polycrystalline copper foil (99.999%, Alfa Aesar). The double layer capacitance (C_{DL}) was found by performing cyclic voltammetry of the electrodes in 0.1M $HClO_4$ in a H-cell. The electrodes were scanned at scan rates of 10-100 mV/s in the potential region of no Faradaic current, and the observed current was plotted vs. scan rate to obtain the double layer capacitance. The ECSA was then calculated using the C_{DL} for the copper foil.

In-situ X-ray adsorption spectroscopy (XAS) was performed at Beamline 5 BM-D at the Advanced Photon Source (APS) at Argonne National Laboratory through the general user program. The XAS data was processed using the IFEFFIT package, including Athena and Artemis.[61] A modified two-compartment H-type electrochemical cell made from acrylic was used for *in-situ* XAS experiments and is shown in (Supplementary Fig. 3). The electrolysis was performed in 0.1M potassium hydroxide under a flowing atmosphere of 5 sccm carbon monoxide. The OD-Cu electrodes were reduced at 10 mA/cm^2, and then held at potentials ranging from -0.2V to -0.5V vs. RHE.

Flow Cell Electrolysis

CO and CO_2 electrolysis were performed in a three-channel flow cell with channels of dimension 2 × 0.5 × 0.15 cm^3. The flow cell design was modified based on engineering drawings kindly provided by Dr. Paul Kenis at University of Illinois at Urbana-Champaign (USA). The electrolytes were aqueous solutions of potassium hydroxide (99.99%, Sigma Aldrich). The gas flow rate into the flow cell was controlled at 10 sccm via a Brooks GF40 mass flow controller. The catholyte and anolyte flow rates were controlled via a peristaltic pump, with the catholyte flow rate ranging from 0.1-1 mL/min depending on the current density (lower flow rates were used at lower current densities to allow for sufficient accumulation of liquid products). The anolyte flow rate was 5 mL/min. The cathode and anode were separated via a hydroxide exchange membrane (FAA-3,

Fumatech). The backpressure of the gas in the flow cell was controlled to atmospheric pressure using a backpressure controller (Cole-Parmer).

Chronopotentiometry experiments were performed using an Autolab PG128N. For the 3-electrode set-up experiments, the cathode potential was measured using an external Ag/AgCl reference electrode (Pine Research). The resistance between the cathode and reference electrode was measured using the current-interrupt technique prior to each applied current density, and the measured applied potential was IR corrected following electrolysis. For each data point, the cell was allowed to reach steady state, and products were quantified over a 300s period. At least three replicates were performed at each current density. For the CO/CO_2 gas switching experiments where the cell voltage is recorded over time, the voltage data were smoothed using the Savitzsky-Golay method to reduce oscillations due to bubble formation at the anode.

Gas products were quantified using a Multigas #5 GC (SRI Instruments) equipped with a Hayesep D and Molsieve 5A columns connected to a thermal conductivity detector (TCD) and a Hayesep D column connected to a flame ionization detector (FID). Hydrogen was quantified using TCD, while ethylene, carbon monoxide (for CO_2 electrolysis), and methane were detected on both FID and TCD. The Faradaic efficiency for products was calculated using the following formula:

$$FE\ (\%) = \frac{nFxV}{j_{Tot}} * 100 \quad (1)$$

where n = # of electrons transferred
F = Faraday's constant
x = mole fraction of product
V = total molar flow rate of gas
j_{Tot} = total current

Liquid products were quantified using a Bruker AVIII 600 MHz NMR spectrometer. Typically, 500 μL of collected catholyte exiting the reactor was mixed with 100 μL D_2O containing 20 ppm (m/m) dimethyl sulphoxide (≥99.9%, Alfa Aesar) as the internal standard. The one-dimensional ^1H spectrum was measured with water suppression using a pre-saturation method.

Labelled $C^{18}O$ experiment

A low pressure $C^{18}O$ lecture bottle (Sigma Aldrich, 95 at% ^{18}O) was used for all labelled experiments. A 30 mL syringe was used to extract the $C^{18}O$ gas and a syringe pump was used to feed the gas into the flow cell at 5 mL/min. Electrolysis was conducted at constant current of 300 mA/cm^2 for 5 minutes and the catholyte was collected for analysis. The liquid products were acidified in an ice bath with hydrochloric acid to a pH value of ~2. Acidification did not affect the mass spectrum analysis, other than allowing for the detection of acetate through acetic acid. Identification of the liquid products was performed using an integrated gas chromatography-mass spectrometry (GC-MS, Agilent 59771A) system. The GC (Agilent 7890B) was equipped with a DB-FFAP column and interfaced directly to the MS (Agilent 59771A). Identification of the GC-MS spectral features were accomplished by comparing the mass fragmentation patterns with those of the NIST library and focused on the shifts of the parent ion of the molecules.

Data Availability

The data that support the findings of this study are available from the corresponding author upon reasonable request.

References

1 Haegel, N. M. *et al.* Terawatt-scale photovoltaics: Trajectories and challenges. *Science* **356**, 141-143, (2017).

2 Herron, J. A., Kim, J., Upadhye, A. A., Huber, G. W. & Maravelias, C. T. A general framework for the assessment of solar fuel technologies. *Energy Environ. Sci.* **8**, 126-157, (2015).

3 Whipple, D. T. & Kenis, P. J. Prospects of CO_2 utilization via direct heterogeneous electrochemical reduction. *J. Phys. Chem. Lett.* **1**, 3451-3458, (2010).

4 Gu, S., Xu, B. & Yan, Y. Electrochemical energy engineering: a new frontier of chemical engineering innovation. *Annu. Rev. Chem. Biomol. Eng.* **5**, 429-454, (2014).

5 Martín, A. J., Larrazábal, G. O. & Pérez-Ramírez, J. Towards sustainable fuels and chemicals through the electrochemical reduction of CO_2: lessons from water electrolysis. *Green Chem.* **17**, 5114-5130, (2015).

6 Jouny, M., Luc, W. & Jiao, F. General Techno-Economic Analysis of CO_2 Electrolysis Systems. *Ind. Eng. Chem. Res.* **57**, 2165-2177, (2018).

7 Jhong, H.-R. M., Ma, S. & Kenis, P. J. A. Electrochemical conversion of CO_2 to useful chemicals: current status, remaining challenges, and future opportunities. *Curr. Opin. Chem. Eng.* **2**, 191-199, (2013).

8 Liu, X. *et al.* Understanding trends in electrochemical carbon dioxide reduction rates. *Nat. Commun.* **8**, 15438, (2017).

9 Montoya, J. H., Shi, C., Chan, K. & Norskov, J. K. Theoretical Insights into a CO Dimerization Mechanism in CO_2 Electroreduction. *J. Phys. Chem. Lett.* **6**, 2032-2037, (2015).

10 Huang, Y., Handoko, A. D., Hirunsit, P. & Yeo, B. S. Electrochemical Reduction of CO_2 Using Copper Single-Crystal Surfaces: Effects of CO* Coverage on the Selective Formation of Ethylene. *ACS Catal.* **7**, 1749-1756, (2017).

11 Verma, S., Lu, X., Ma, S., Masel, R. I. & Kenis, P. J. A. The effect of electrolyte composition on the electroreduction of CO_2 to CO on Ag based gas diffusion electrodes. *PCCP* **18**, 7075-7084, (2016).

12 Xiao, H., Cheng, T., Goddard, W. A., 3rd & Sundararaman, R. Mechanistic Explanation of the pH Dependence and Onset Potentials for Hydrocarbon Products from Electrochemical Reduction of CO on Cu (111). *J. Am. Chem. Soc.* **138**, 483-486, (2016).

13 Dinh, C.-T. *et al.* CO_2 electroreduction to ethylene via hydroxide-mediated copper catalysis at an abrupt interface. *Science* **360**, 783-787, (2018).

14 Verma, S. *et al.* Insights into the Low Overpotential Electroreduction of CO_2 to CO on a Supported Gold Catalyst in an Alkaline Flow Electrolyzer. *ACS Energy Lett.* **3**, 193-198, (2018).

15 Spurgeon, J. M. & Kumar, B. A comparative technoeconomic analysis of pathways for commercial electrochemical CO_2 reduction to liquid products. *Energy Environ. Sci.* **11**, 1536-1551, (2018).

16 Reske, R., Mistry, H., Behafarid, F., Roldan Cuenya, B. & Strasser, P. Particle size effects in the catalytic electroreduction of CO_2 on Cu nanoparticles. *J. Am. Chem. Soc.* **136**, 6978-6986, (2014).

17 Loiudice, A. *et al.* Tailoring copper nanocrystals towards C_2 products in electrochemical CO_2 reduction. *Angew. Chem. Int. Ed.* **55**, 5789-5792, (2016).

18 Baturina, O. A. *et al.* CO_2 Electroreduction to Hydrocarbons on Carbon-Supported Cu Nanoparticles. *ACS Catal.* **4**, 3682-3695, (2014).

19 Kas, R. *et al.* Three-dimensional porous hollow fibre copper electrodes for efficient and high-rate electrochemical carbon dioxide reduction. *Nat. Commun.* **7**, 10748, (2016).

20 Sen, S., Liu, D. & Palmore, G. T. R. Electrochemical Reduction of CO_2 at Copper Nanofoams. *ACS Catal.* **4**, 3091-3095, (2014).

21 Rahaman, M., Dutta, A., Zanetti, A. & Broekmann, P. Electrochemical Reduction of CO_2 into Multicarbon Alcohols on Activated Cu Mesh Catalysts: An Identical Location (IL) Study. *ACS Catal.* **7**, 7946-7956, (2017).

22 Dutta, A., Rahaman, M., Luedi, N. C., Mohos, M. & Broekmann, P. Morphology Matters: Tuning the Product Distribution of CO_2 Electroreduction on Oxide-Derived Cu Foam Catalysts. *ACS Catal.* **6**, 3804-3814, (2016).

23 Hahn, C. *et al.* Engineering Cu surfaces for the electrocatalytic conversion of CO_2: Controlling selectivity toward oxygenates and hydrocarbons. *PNAS* **114**, 5918, (2017).

24 Kim, Y.-G., Javier, A., Baricuatro, J. H. & Soriaga, M. P. Regulating the Product Distribution of CO Reduction by the Atomic-Level Structural Modification of the Cu Electrode Surface. *Electrocatalysis* **7**, 391-399, (2016).

25 Clark, E. L., Hahn, C., Jaramillo, T. F. & Bell, A. T. Electrochemical CO_2 Reduction over Compressively Strained CuAg Surface Alloys with Enhanced Multi-Carbon Oxygenate Selectivity. *J. Am. Chem. Soc.* **139**, 15848-15857, (2017).

26 Ren, D., Ang, B. S.-H. & Yeo, B. S. Tuning the Selectivity of Carbon Dioxide Electroreduction toward Ethanol on Oxide-Derived Cu_xZn Catalysts. *ACS Catal.* **6**, 8239-8247, (2016).

27 Zhang, S. *et al.* Polymer-supported CuPd nanoalloy as a synergistic catalyst for electrocatalytic reduction of carbon dioxide to methane. *PNAS* **112**, 15809-15814, (2015).

28 Sarfraz, S., Garcia-Esparza, A. T., Jedidi, A., Cavallo, L. & Takanabe, K. Cu–Sn Bimetallic Catalyst for Selective Aqueous Electroreduction of CO_2 to CO. *ACS Catal.* **6**, 2842-2851, (2016).

29 Lee, S., Park, G. & Lee, J. Importance of Ag–Cu Biphasic Boundaries for Selective Electrochemical Reduction of CO_2 to Ethanol. *ACS Catal.* **7**, 8594-8604, (2017).

30 Mistry, H. *et al.* Highly selective plasma-activated copper catalysts for carbon dioxide reduction to ethylene. *Nat. Commun.* **7**, 12123, (2016).

31 Jiang, K. *et al.* Metal ion cycling of Cu foil for selective C–C coupling in electrochemical CO_2 reduction. *Nat. Catal.* **1**, 111-119, (2018).

32 Gao, D. *et al.* Plasma-Activated Copper Nanocube Catalysts for Efficient Carbon Dioxide Electroreduction to Hydrocarbons and Alcohols. *ACS Nano* **11**, 4825-4831, (2017).

33 Handoko, A. D. *et al.* Mechanistic Insights into the Selective Electroreduction of Carbon Dioxide to Ethylene on Cu_2O-Derived Copper Catalysts. *J. Phys. Chem. C* **120**, 20058-20067, (2016).

34 Tang, W. *et al.* The importance of surface morphology in controlling the selectivity of polycrystalline copper for CO_2 electroreduction. *PCCP* **14**, 76-81, (2012).

35 Li, C. W., Ciston, J. & Kanan, M. W. Electroreduction of carbon monoxide to liquid fuel on oxide-derived nanocrystalline copper. *Nature* **508**, 504-507, (2014).

36 Bertheussen, E. *et al.* Acetaldehyde as an Intermediate in the Electroreduction of Carbon Monoxide to Ethanol on Oxide-Derived Copper. *Angew. Chem. Int. Ed.* **55**, 1450-1454, (2016).

37 Raciti, D. *et al.* Low-Overpotential Electroreduction of Carbon Monoxide Using Copper Nanowires. *ACS Catal.* **7**, 4467-4472, (2017).

38 Feng, X., Jiang, K., Fan, S. & Kanan, M. W. A Direct Grain-Boundary-Activity Correlation for CO Electroreduction on Cu Nanoparticles. *ACS Cent. Sci.* **2**, 169-174, (2016).

39 Verdaguer-Casadevall, A. *et al.* Probing the Active Surface Sites for CO Reduction on Oxide-Derived Copper Electrocatalysts. *J. Am. Chem. Soc.* **137**, 9808-9811, (2015).

40 Mariano, R. G., McKelvey, K., White, H. S. & Kanan, M. W. Selective increase in CO_2 electroreduction activity at grain-boundary surface terminations. *Science* **358**, 1187-1192, (2017).

41 Raciti, D. *et al.* Low-Overpotential Electroreduction of Carbon Monoxide Using Copper Nanowires. *ACS Catal.* **7**, 4467-4472, (2017).

42 Raciti, D. & Wang, C. Recent Advances in CO_2 Reduction Electrocatalysis on Copper. *ACS Energy Lett.* **3**, 1545-1556, (2018).

43 Eren, B. *et al.* Activation of Cu(111) surface by decomposition into nanoclusters driven by CO adsorption. *Science* **351**, 475-478, (2016).

44 Eren, B. *et al.* One-dimensional nanoclustering of the Cu(100) surface under CO gas in the mbar pressure range. *Surf. Sci.* **651**, 210-214, (2016).

45 Gunathunge, C. M. *et al.* Spectroscopic Observation of Reversible Surface Reconstruction of Copper Electrodes under CO_2 Reduction. *J. Phys. Chem. C* **121**, 12337-12344, (2017).

46 Kuhl, K. P., Cave, E. R., Abram, D. N. & Jaramillo, T. F. New insights into the electrochemical reduction of carbon dioxide on metallic copper surfaces. *Energy Environ. Sci.* **5**, 7050-7059, (2012).

47 Gupta, N., Gattrell, M. & MacDougall, B. Calculation for the cathode surface concentrations in the electrochemical reduction of CO_2 in $KHCO_3$ solutions. *J. Appl. Electrochem.* **36**, 161-172, (2006).

48 Ma, S. *et al.* Carbon nanotube containing Ag catalyst layers for efficient and selective reduction of carbon dioxide. *J. Mater. Chem. A* **4**, 8573-8578, (2016).

49 Hoang, T. T. H., Ma, S., Gold, J. I., Kenis, P. J. A. & Gewirth, A. A. Nanoporous Copper Films by Additive-Controlled Electrodeposition: CO_2 Reduction Catalysis. *ACS Catal.* **7**, 3313-3321, (2017).

50 Birdja, Y. Y. & Koper, M. T. The Importance of Cannizzaro-Type Reactions during Electrocatalytic Reduction of Carbon Dioxide. *J. Am. Chem. Soc.* **139**, 2030-2034, (2017).

51 Garza, A. J., Bell, A. T. & Head-Gordon, M. Mechanism of CO_2 Reduction at Copper Surfaces: Pathways to C_2 Products. *ACS Catal.* **8**, 1490-1499, (2018).

52 Greenzaid, P., Luz, Z. & Samuel, D. A nuclear magnetic resonance study of the reversible hydration of aliphatic aldehydes and ketones. II. The acid-catalyzed oxygen exchange of acetaldehyde. *J. Am. Chem. Soc.* **89**, 756-759, (1967).

53 Clark, E. L. & Bell, A. T. Direct Observation of the Local Reaction Environment during the Electrochemical Reduction of CO_2. *J. Am. Chem. Soc.* **140**, 7012-7020, (2018).
54 Gileadi, E. *Physical electrochemistry: fundamentals, techniques and applications*. (2011).
55 Hori, Y., Takahashi, I., Koga, O. & Hoshi, N. Electrochemical reduction of carbon dioxide at various series of copper single crystal electrodes. *J. Mol. Catal. A: Chem.* **199**, 39-47, (2003).
56 Song, Y. *et al.* High-Selectivity Electrochemical Conversion of CO_2 to Ethanol using a Copper Nanoparticle/N-Doped Graphene Electrode. *ChemistrySelect* **1**, 6055-6061, (2016).
57 Ren, D. *et al.* Selective Electrochemical Reduction of Carbon Dioxide to Ethylene and Ethanol on Copper(I) Oxide Catalysts. *ACS Catal.* **5**, 2814-2821, (2015).
58 Weng, Z. *et al.* Electrochemical CO_2 Reduction to Hydrocarbons on a Heterogeneous Molecular Cu Catalyst in Aqueous Solution. *J. Am. Chem. Soc.* **138**, 8076-8079, (2016).
59 De Luna, P. *et al.* Catalyst electro-redeposition controls morphology and oxidation state for selective carbon dioxide reduction. *Nat. Catal.* **1**, 103-110, (2018).
60 Hoang, T. T. H. *et al.* Nanoporous Copper–Silver Alloys by Additive-Controlled Electrodeposition for the Selective Electroreduction of CO_2 to Ethylene and Ethanol. *J. Am. Chem. Soc.* **140**, 5791-5797, (2018).
61 Ravel, B. & Newville, M. ATHENA, ARTEMIS, HEPHAESTUS: data analysis for X-ray absorption spectroscopy using IFEFFIT. *J. Synchrotron Radiat.* **12**, 537-541, (2005).

Acknowledgements

We would like to thank Dr. Bingjun Xu and Marco Dunwell for useful discussion. We would also like to thank Brian Murphy for help with GC-MS experiments and Dr. Brian Setzler for help with the transport model. This material is based upon work supported by the Department of Energy under Award Number DE-FE0029868. The authors also thank the National Science Foundation Faculty Early Career Development program (Award No. CBET-1350911). This research used resources of the Advanced Photon Source, a U.S. Department of Energy (DOE) Office of Science User Facility operated for the DOE Office of Science by Argonne National Laboratory under Contract No. DE-AC02-06CH11357**.**

Author contributions

M.J. synthesized the electrodes, performed XAS characterization, designed and performed flow electrolysis experiments, analysed the data, and wrote the manuscript. W.L. performed SEM, XPS, and XRD characterizations and surface pH calculations. F.J. supervised the project. All authors contributed to discussion of results and manuscript preparation.

Competing interests

The authors declare no competing financial interests.